PERGAMON

International Journal of Heat and Mass Transfer 42 (1999) 1935–1944

International Journal of HEAT and MASS TRANSFER

Heat transfer and pressure drop during condensation of refrigerant 134a in an axially grooved tube

D. Graham, J.C. Chato, T.A. Newell*

Air Conditioning and Refrigeration Center, Department of Mechanical and Industrial Engineering, University of Illinois, 1206 W. Green St., Urbana, IL 61801, U.S.A.

Received 25 July 1997; in final form 3 September 1998

Abstract

Condensation experiments have been performed over a mass flux range of 75–450 kg m^{-2} s^{-1} in an 8.91 mm inside diameter, axially grooved, micro-fin tube with R134a. At 75 kg m^{-2} s^{-1}, the axially grooved tube performs marginally better than a smooth tube, but worse than a similarly grooved tube with an 18° helix angle. Mass fluxes at 150 kg m^{-2} s^{-1} and greater show broad quality ranges in which the axially grooved tube performs significantly better than both smooth and helically grooved tubes. Pressure drop characteristics of the axially grooved tube are similar to those found in an 18° helix angle tube.

Nomenclature

c_p specific heat at constant pressure
c_p,l specific heat at constant pressure for liquid refrigerant
D diameter
$D_{eq,flow}$ equivalent flow diameter
EF enhancement factor
f_L liquid friction factor, equation (15)
Fr_l liquid-only Froude number $(G/\rho_l)^2/gD$
Fr_{so} Soliman's modified Froude number, equations (8) and (9)
Ft Froude rate parameter, equations (18) and (19)
G mass flux
g gravitational acceleration
Ga Galileo number, $\rho_l(\rho_l-\rho_v)D^3/\mu_l^2$
i_{lv} enthalpy of vaporization
Ja Jakob number, $c_p(T_{sat}-T_s)/i_{lv}$
k thermal conductivity
k_l liquid thermal conductivity
$\dot{m}$ mass flow rate
m_l liquid mass flow rate
m_v vapor mass flow rate
Nu Nusselt number
PF penalty factor
Pr Prandtl number, $\mu c_p/k$
Pr_l liquid Prandtl number, $\mu c_{p,l}/k_l$
Re_l liquid Reynolds number, $GD(1-x)/\mu_l$
Re_{vo} vapor only Reynolds number, GD/μ_v
V_v vapor velocity
x quality
x_i inlet quality
x_o outlet quality
X_{tt} Lockhart–Martinelli number, equation (6).

Greek symbols

α void fraction
α_i inlet void fraction
α_o outlet void fraction
ΔP pressure drop
ΔP_{ACC} acceleration pressure drop, equation (13)
ΔP_{FRIC} frictional pressure drop, equation (12)
μ viscosity
μ_l liquid viscosity
μ_v vapor viscosity
ρ_v vapor density
ρ_l liquid density
ϕ_l^2 two-phase pressure drop multiplier.

1. Introduction

Enhancement of tube heat transfer without an equivalent increase of pressure drop is an active area of inves-

* Corresponding author. Tel.: 001 217 333 1655; fax: 001 217 333 1942; e-mail: t-newell@uiuc.edu

0017–9310/99/$ - see front matter
PII: S0017–9310(98)00307–X

tigation in the refrigeration and air conditioning fields [1–14]. 'Micro-fin' enhancements are of special interest because little, if any, additional material is required for inscribing the internal tube surface with structures that can result in high heat transfer increases. Most studies have investigated 'helical' micro-fin tubes [4, 6–14] that are more readily available commercially.

Chiang [1] found axial grooved tubes to generally show higher performance than helical tubes over a broad range of mass fluxes and qualities for both evaporation and condensation. Direct comparison between the axial grooved tubes and helical (18°) grooved tubes could not be made because the grooves were of significantly different fin geometries and fin frequencies. The 10 mm diameter tubes had 72 and 60 internal fins for the axial and 18° helix grooves, respectively. For the 7.5 mm diameter tubes, Chiang [1] tested 60 fins for the axial and 43 internal fins for the 18° helix groove configuration.

In the present study, a custom fabricated 8.91 mm diameter tube with 60 axial fins was obtained. The fin geometry and number of fins geometrically matches an 18° helix tube made by the manufacturer. The 18° helix tube was previously tested at the University of Illinois Air Conditioning and Refrigeration Center's (ACRC) condenser test facility [6, 7]. Investigation of the geometrically similar, axially grooved tube has been undertaken in order to examine trends and performance differences in a detailed manner over a range of refrigerant mass fluxes and qualities.

2. Background

An apparatus has been designed in the ACRC at the University of Illinois that allows in-tube condensation data to be collected over a wide range of operating conditions. In the test-condenser, average 'local', in-tube heat transfer coefficients and pressure drops of the working fluid are measured. A schematic of the apparatus is provided in Fig. 1. Detailed discussion of measurement techniques, accuracy and uncertainty are contained in Dobson [2].

The refrigerant is circulated through the refrigerant loop by a MicroPump three gear, variable speed pump. The mass flux of the refrigerant is measured immediately after the pump, either by a Micro-Motion D mass flow meter for flow rates less than 0.90 kg min^{-1}, or a Max Machinery positive displacement flow meter for flow rates higher than 0.90 kg min^{-1}.

After the pump, the refrigerant is set to the desired condition by the use of a preheater, consisting of a 9.52 mm o.d. copper tube. Each pass of the tube is wrapped with resistance heater tapes that are used to input heat to the refrigerant. This allows the experimenter to set the temperature and quality of the refrigerant at the test section inlet. Located systematically throughout the test section are thermocouples which measure the wall temperatures. The thermocouples are staggered in such a way as to measure circumferential and longitudinal temperature distributions at the tube wall. Temperatures were measured with thermocouples that were calibrated with a constant temperature bath, which was found to have an uncertainty of 0.1°C.

Located across the test section is a differential pressure transducer, which measures the pressure drop in a length of 1.22 m. The uncertainty of this transducer was estimated to be ± 1 kPa. Absolute pressure transducers are also located at the test section inlet, the test section outlet, at the receiver and before the preheater. These transducers were calibrated together on a dead weight tester over their range of applicability. From these tests, the uncertainty of these instruments is estimated at ± 7 kPa.

After the refrigerant leaves the test section, it is cooled to a subcooled liquid. The refrigerant then passes through a filter and is recirculated through the pump. The temperature of the refrigerant is in part controlled by the heat input from the preheater to the test section, but the majority of the temperature control is obtained by the use of a heated water tank. A refrigerant receiver is placed into this tank, and by varying the temperature of the water in this tank, and the amount of refrigerant that flows through this receiver, the system pressure can be set to the necessary quantity.

Water is used to condense the refrigerant in the test section. The temperature of the water is varied by the use of a water heater. After the heater, the water enters an annulus that is centered around the test section. This annulus is made with a 19.1 mm o.d. plastic tube. Inside the tube are a series of plastic mixers that are used to swirl the flow, and maintain a nearly uniform temperature at any longitudinal location. The water flow rate is measured at the discharge with a graduated cylinder and a stopwatch. The entire experimental apparatus including the test section, water section and all the tubing is covered with insulation to minimize losses to the environment.

The experiments were all run at a saturation temperature of approximately 35°C. Once the desired conditions have been set, and steady state is achieved, data is collected for 5 min. Calculation of the heat transfer coefficient is made by using a cooling water energy balance with the overall temperature difference between the tube wall and refrigerant. The tube wall temperature is an area weighted averaged of thermocouples mounted in the tube wall over the length of the tube. The refrigerant temperature is the average of the inlet and outlet refrigerant temperatures. Details of thermocouple mounting procedures are described by Dobson [2]. The test section outlet quality is determined from an energy balance of the test section and the inlet quality. The local quality is defined as the average of the inlet and outlet qualities. At low mass fluxes (75 kg m^{-2} s^{-1}), the difference between inlet and outlet qualities ranged from 0.15 to 0.30. At the

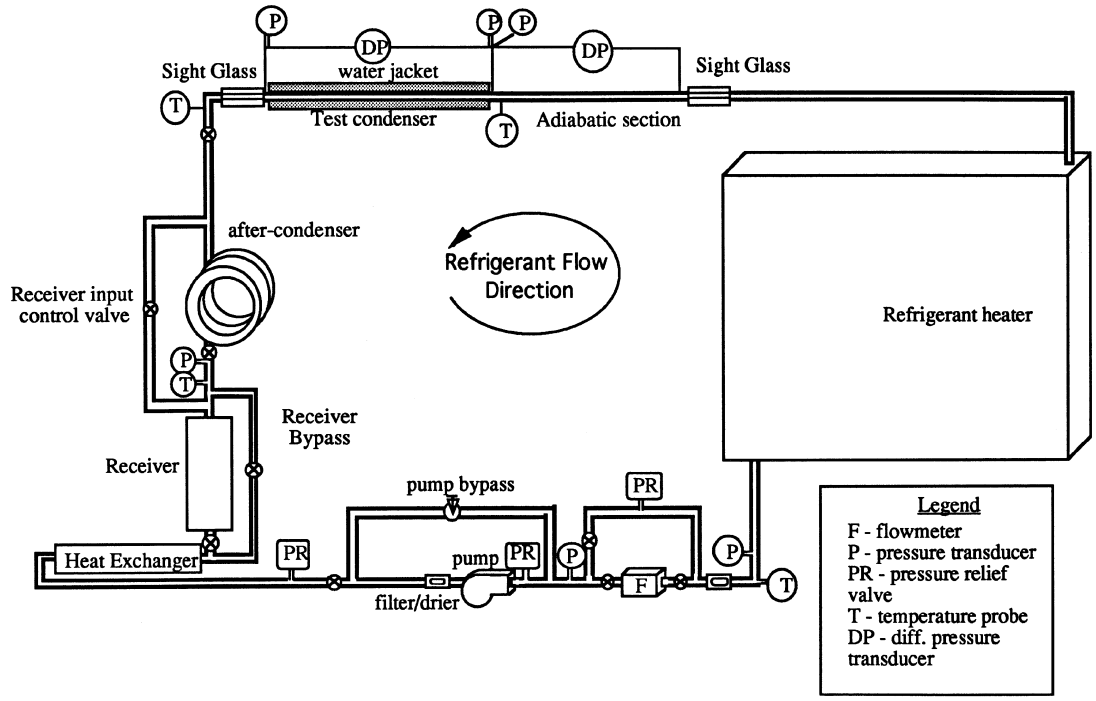

Fig. 1. Experimental apparatus [2].

high mass flux range (450 kg m^{-2} s^{-1}), the difference between inlet and outlet qualities over the range of test conditions was between 0.10 and 0.20. Temperature differences between the tube wall and the refrigerant were generally between 2 and 8°C.

The test section used in this study is a 9.52 mm o.d. tube, which contains 60 trapezoidal fins that are arranged axially inside the tube at an angle of 0° to the axial direction. The maximum inside diameter of the tube is 8.91 mm and the minimum inside diameter is 8.53 mm. The fins have an average height of 0.180 mm. Experiments run by Ponchner [7] are also included in this report. Ponchner's experiments were run on the same apparatus and his test section differed from the current test section only by the fact that its 60 trapezoidal fins were arranged helically inside the tube at an angle of 18°. Figure 2 shows the cross section of the microfinned tube used in this study and the one used by Ponchner [7].

In this study two parameters are used to compare the performance of the microfinned tubes to the performance of a similar smooth tube. The first parameter compares the heat transfer characteristics, while the second compares the pressure drop characteristics. The inside surface area of the microfinned tubes was measured by making measurements with a microscope. The microfinned tubes have an internal surface area that is 1.62 times the area

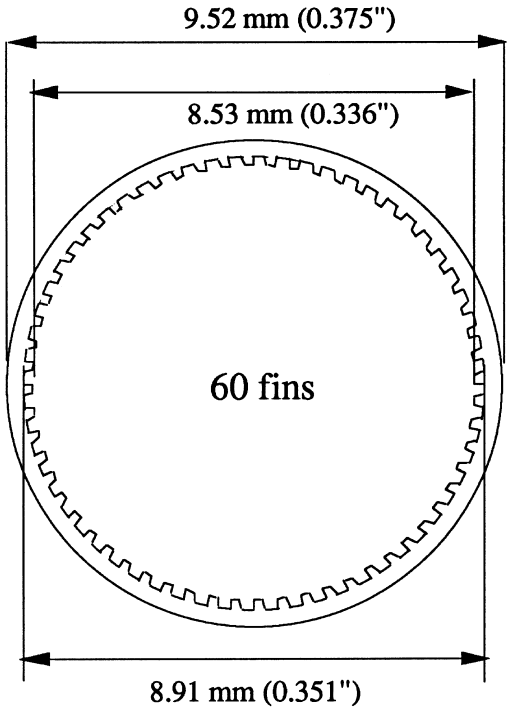

Fig. 2. Cross-sectional view of the microfinned test sections.

of a smooth tube with a diameter equal to that diameter from the base of the grooves (8.91 mm).

The parameter used to compare the heat transfer characteristics is the enhancement factor, *EF*. For the purpose of this study, the enhancement factor is defined to be the ratio of the heat transfer of the enhanced tube to the heat transfer of a similar smooth tube, operating at the same conditions.

$$EF = \left(\frac{\dot{Q}_{\text{microfin}}}{\dot{Q}_{\text{smooth}}}\right)_{\text{same conditions}}.$$

Here the heat transfer rate for the two tube geometries can be defined with the following equations:

$$\dot{Q}_{\text{microfin}} = h_{\text{microfin}} A_{\text{microfin}} \Delta T$$

$$\dot{Q}_{\text{smooth}} = h_{\text{smooth}} A_{\text{smooth}} \Delta T.$$

At equivalent temperature differences, the enhancement factor can be represented as the heat transfer enhancement multiplied by the area ratio. If the area of the smooth tube is taken as the area of a smooth tube with an inside diameter equal to the maximum inside diameter of the microfinned tubes, the area ratio becomes 1.62.

$$EF = \left(\frac{h_{\text{microfin}}}{h_{\text{smooth}}}\right) A_{\text{rat}} = 1.62\left(\frac{h_{\text{microfin}}}{h_{\text{smooth}}}\right). \tag{1}$$

The heat transfer coefficient for the comparable smooth tube was calculated using a Dobson correlation [2, 3], which is divided into a wavy flow correlation and an annular flow correlation. The form of the annular correlation is the following:

$$Nu = 0.023 Re_{\text{l}}^{0.8} Pr_{\text{l}}^{0.4}\left[1 + \frac{2.22}{X_{\text{u}}^{0.889}}\right]. \tag{2}$$

The wavy correlation is as follows:

$$Nu = \frac{0.23 Re_{\text{vo}}^{0.12}}{1 + 1.11 X_{\text{tt}}^{0.58}}\left[\frac{GaPr}{Ja}\right]^{0.25} + (1 - \theta_1/\pi) Nu_{\text{forced}} \tag{3}$$

where θ_1 = angle subtended from the top of the tube to the liquid level

$$Nu_{\text{forced}} = 0.0195 Re_{\text{l}}^{0.8} Pr_{\text{l}}^{0.4} \phi_{\text{l}}(X_{\text{u}}) \tag{4}$$

and:

$$\phi_{\text{l}}(X_{\text{u}}) = \sqrt{1.376 + \frac{c_1}{X_{\text{tt}}^{c_2}}} \tag{5}$$

The turbulent-turbulent Lockhart–Martinelli parameter [15] can be calculated by:

$$X_{\text{u}} = \left(\frac{\rho_{\text{v}}}{\rho_{\text{l}}}\right)^{0.5}\left(\frac{\mu_{\text{l}}}{\mu_{\text{v}}}\right)^{0.1}\left(\frac{1-x}{x}\right)^{0.9}. \tag{6}$$

For $0 < Fr_{\text{l}} \leqslant 0.7$:

$$c_1 = 4.172 + 5.48 Fr_{\text{l}} - 1.564 Fr_{\text{l}}^2$$

$$c_2 = 1.773 - 0.169 Fr_{\text{l}}$$

For $Fr_{\text{l}} > 0.7$:

$$c_1 = 7.242$$

$$c_2 = 1.6555$$

The liquid level angle, θ_1, can be related to the void fraction by the following equation, if the area occupied by the condensate film is neglected:

$$\alpha = \frac{\theta_1}{\pi} - \frac{\sin(2\theta_1)}{2\pi}. \tag{7}$$

Dobson [2, 3] also recommended the conditions under which each of the correlations should be used. The parameter used to predict the flow regime is the Froude number, as defined by Soliman [16]. For a $Fr_{\text{so}} < 20$, Dobson [2, 3] recommends that the wavy correlation be used and for $Fr_{\text{so}} > 20$ Dobson [2, 3] recommends that the annular form of the correlation be used where:

$$Fr_{\text{so}} = 0.025 Re_{\text{l}}^{1.59}\left(\frac{1 + 1.09 X_{\text{tt}}^{0.039}}{X_{\text{tt}}}\right)^{1.5}\frac{1}{Ga^{0.5}} \quad \text{for } Re_{\text{l}} \leqslant 1250 \tag{8}$$

$$Fr_{\text{so}} = 1.26 Re_{\text{l}}^{1.04}\left(\frac{1 + 1.09 X_{\text{tt}}^{0.039}}{X_{\text{tt}}}\right)^{1.5}\frac{1}{Ga^{0.5}} \quad \text{for } Re_{\text{l}} > 1250. \tag{9}$$

Along with the heat transfer enhancement of the microfinned tube, there is also a penalty factor due to the increased pressure drop generated by the fins. Here the penalty factor, *PF*, is defined as the ratio of the pressure drop found in the microfinned tube to the pressure drop of a similar smooth tube operating at the same conditions, over the same length.

$$PF = \left(\frac{\Delta P_{\text{microfin}}}{\Delta P_{\text{smooth}}}\right)_{\text{equal length}} \tag{10}$$

The corresponding pressure drop for the smooth tube was calculated using the correlation proposed by Souza [17, 18]. This correlation takes into account both frictional and acceleration pressure drops and is defined as:

$$\Delta P_{\text{SMOOTH}} = \Delta P_{\text{ACC}} + \Delta P_{\text{FRIC}} \tag{11}$$

$$\Delta P_{\text{FRIC}} = \Delta P_{\text{L}} \phi_{\text{l}}^2 \tag{12}$$

$$\Delta P_{\text{ACC}} = \frac{16\dot{m}^2}{\pi^2 D^4}\left\{\left[\frac{x_{\text{o}}^2}{\rho_{\text{v}}\alpha_{\text{o}}} + \frac{(1-x_{\text{o}})^2}{\rho_{\text{l}}(1-\alpha_{\text{o}})}\right] - \left[\frac{x_{\text{i}}^2}{\rho_{\text{v}}\alpha_{\text{i}}} + \frac{(1-x_{\text{i}})^2}{\rho_{\text{l}}(1-\alpha_{\text{i}})}\right]\right\} \tag{13}$$

where

$$\Delta P_{\mathrm{l}} = \frac{2 f_{\mathrm{l}} G^2 (1-x)^2 L}{\rho_{\mathrm{l}} D} \tag{14}$$

$$f_{\mathrm{l}} = \frac{0.079}{Re_{\mathrm{l}}^{0.25}}. \tag{15}$$

The void fraction (α) can be calculated using the Zivi [19] correlation:

$$\alpha = \frac{1}{1+\left(\frac{1-x}{x}\right)\left(\frac{\rho_{\mathrm{v}}}{\rho_{\mathrm{l}}}\right)^{0.67}}. \tag{16}$$

It should be noted that the smooth tube diameter used in the above calculations is an equivalent flow diameter, $D_{\mathrm{eq,flow}}$. The equivalent flow diameter is related to the cross-sectional inside area of the micro-finned tube by the following equation:

$$A_{\mathrm{cross\text{-}sect}} = \frac{\pi}{4}(D_{\mathrm{eq,flow}})^2. \tag{17}$$

3. Results

Trends in the axially grooved tube's heat transfer are shown in Fig. 3 over a range of qualities and for mass fluxes from 75 to 450 kg m^{-2} s^{-1}. With the exception of the 75 kg m^{-2} s^{-1} mass flux condition, the axially grooved tube generally outperformed the 18° helix angle tube. Plotting the axially grooved tube and the 18° helix grooved tube using the enhancement factor defined by equation (1) helps identify important trends in the data.

Figures 4–8 show the axial and 18° helix enhancement factors for each mass flux condition. Ponchner's [6] data has been used for the 18° helix performance. As previously described, a Froude number of 20 was defined by Dobson as the transition between a stratified wavy dominated flow and an annular liquid film flow. High gas velocities, caused by high quality and/or high mass flux conditions, result in the annular film.

An interesting trend shown in Figs 4–8 is the systematic progression of high levels of enhancement for the axially grooved tube as the mass flux changes. At low fluxes the axial tube performs poorly. As the mass flux increases, depending on the quality, increases in heat transfer enhancement significantly above those for the 18° helix tube are observed.

At the lowest mass flux tested, as shown in Fig. 4, the enhancement factor for the axially grooved tube is significantly lower than that of the 18° helix tube. The 18° helix tube shows an enhancement factor somewhat higher than the 62% increase in surface area over a smooth tube's internal surface. The axial grooved tube shows an improvement that is only 20% greater than the smooth tube. All quality conditions for the low mass flux condition are at Froude numbers less than 20. The enhancement factors, therefore, are based on the tube performances relative to the stratified wavy flow heat transfer predictions. The grooves in the axial tube may be inhibiting fluid from draining into a stratified flow configuration. Additionally, with relatively low vapor velocities, liquid may be locked into the grooves, effectively blocking the vapor from interacting with the tube wall surfaces. The helical tube enhancement shows that it may somewhat augment the drainage of liquid refrigerant, thus exposing or allowing more of its surface area to participate in heat transfer.

Increases in mass flux, as shown in Figs 5–8, show regions in which the axial grooved tube's enhancement is significantly higher than the tube's area enhancement effect. At a mass flux of 150 kg m^{-2} s^{-1}, as shown in Fig. 5, the enhancement factor is approximately 2.5 at higher qualities. The Froude number for the conditions shown in Fig. 5 are all below 20, requiring that the stratified wavy flow form of Dobson's relation be used for smooth tube heat transfer predictions. The helical tube shows a relatively consistent level of enhancement that is essentially that due to the 62% surface area enhancement.

Examining Figs 6 and 7 reveals that increasing the mass flux to 225 and 300 kg m^{-2} s^{-1} causes the axial tube region of significant heat transfer enhancement to move toward lower qualities. The helical tube generally shows a relatively steady enhancement factor that remains near the level expected due to its area enhancement. Peak enhancement factors of 2.5 are obtained for the 225 kg m^{-2} s^{-1} mass flux, while the 300 kg m^{-2} s^{-1} mass flux shows enhancements near 2.6. At high qualities, although the heat transfer coefficients have increased relative to lower quality conditions (see Fig. 3), the level of axial tube enhancement relative to a smooth tube has diminished. The region where the enhancement level drops, at a quality of approximately 0.6 in Figs 6 and 7, is where the Froude number is 20, indicating that the flow in a smooth tube would be in an annular flow configuration.

Figure 8 shows a continued progression of the axial tube region of high enhancement moving toward lower qualities as the mass flux continues to increase. The diminished enhancement effect relative to a smooth tube and the helical tube occurs at higher qualities. The drop in enhancement is generally occurring where the Froude number is 20 and the smooth tube flow is transitioning to an annular flow condition. Peak axial tube enhancement factors continue to show higher levels of enhancement. A mass flux of 450 kg m^{-2} s^{-1} shows peak enhancement factors of 2.8. It is interesting to note that the helical tube continues to show an enhancement that generally reflects the area enhancement, rather than the pronounced enhancement effect shown by the axial tube. The helical tube seems to show a flow field configuration that consistently follows that of a smooth tube. That is, the relatively flat enhancement factor over the range of qualities

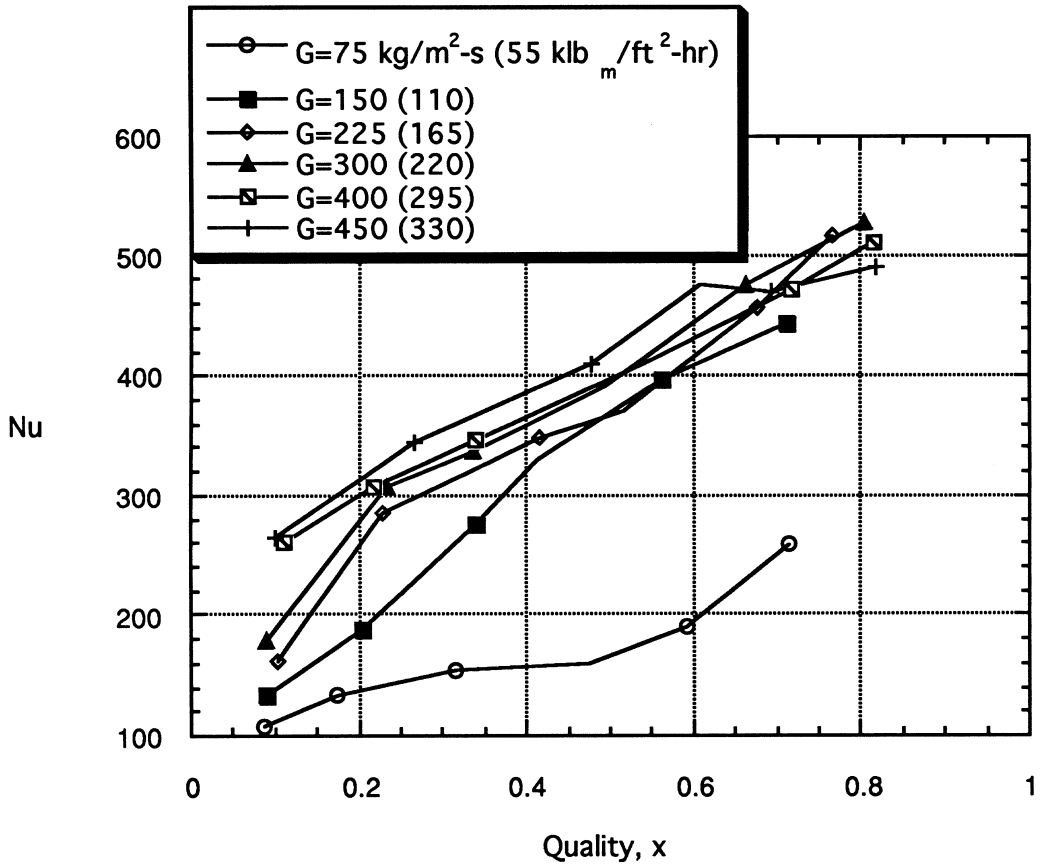

Fig. 3. Heat transfer coefficient versus quality for the axially grooved tube over a range of refrigerant mass fluxes.

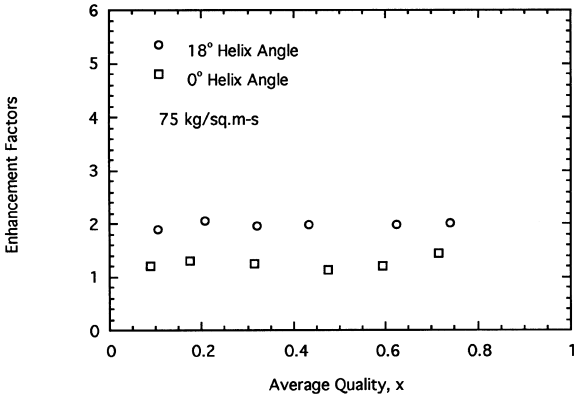

Fig. 4. Enhancement factor for the axial and helical tubes over a range of qualities for a mass flux of 75 kg m^{-2} s^{-1}.

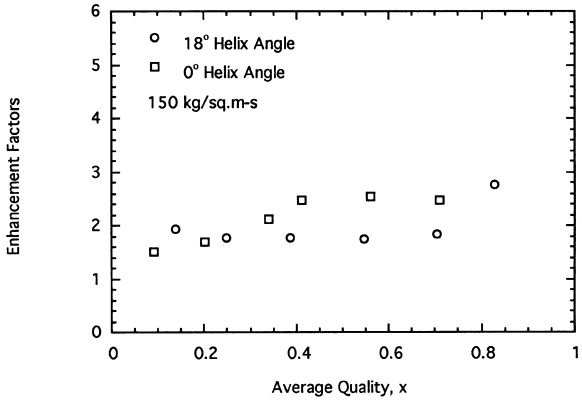

Fig. 5. Enhancement factor for the axial and helical tubes over a range of qualities for a mass flux of 150 kg m^{-2} s^{-1}.

where the smooth tube correlation switches from stratified wavy to annular flow configurations indicates that the helical tube may transition between these flow regions in a similar manner. It should also be noted that at higher mass fluxes and qualities, both axial and helical tubes show a trend toward enhancement levels that are less than their smooth tube area ratios.

Pressure drop characteristics of the axial tube, relative to the helical tube, are shown for two flow conditions in Figs 9 and 10 using the penalty factor defined by equation

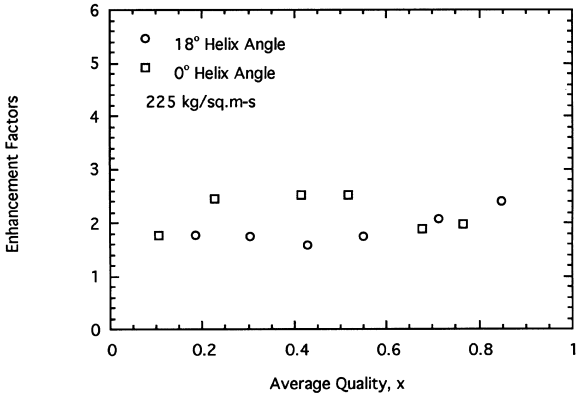

Fig. 6. Enhancement factor for the axial and helical tubes over a range of qualities for a mass flux of 225 kg m^{-2} s^{-1}.

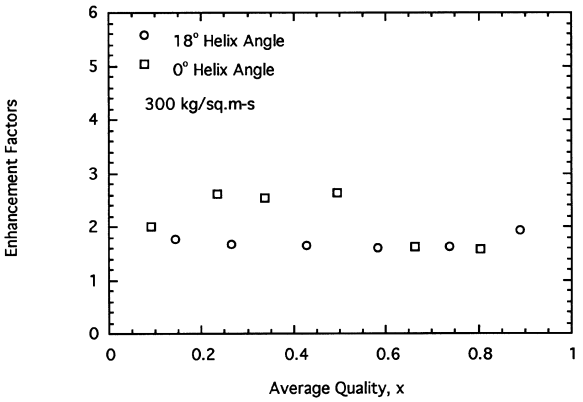

Fig. 7. Enhancement factor for the axial and helical tubes over a range of qualities for a mass flux of 300 kg m^{-2} s^{-1}.

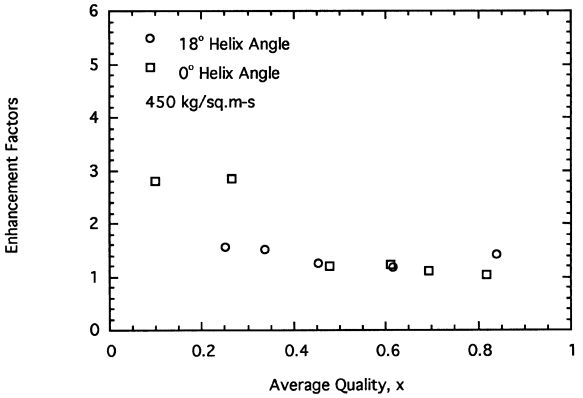

Fig. 8. Enhancement factor for the axial and helical tubes over a range of qualities for a mass flux of 450 kg m^{-2} s^{-1}.

(10). Pressure drop data for mass fluxes below 225 kg m^{-2} s^{-1} are below the level of reliable resolution of the experiment's pressure transducer. Both figures generally

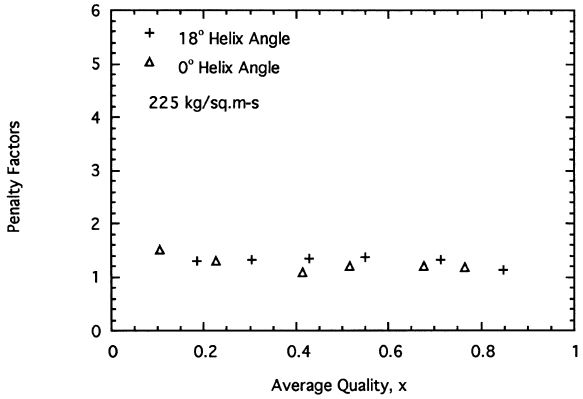

Fig. 9. Penalty factor for the axial and helical tubes over a range of qualities for a mass flux of 225 kg m^{-2} s^{-1}.

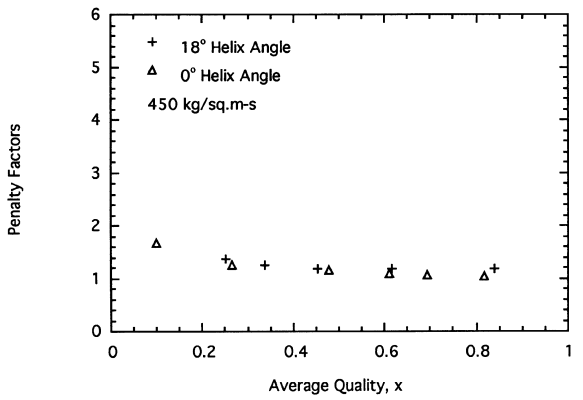

Fig. 10. Penalty factor for the axial and helical tubes over a range of qualities for a mass flux of 450 kg m^{-2} s^{-1}.

show that the micro-fin configuration results in low penalty factors. The most interesting feature of these figures is the similarity in penalty factors for the axial and helical tubes. Even though the axial tube shows significant deviations from the helical tube's characteristics on a heat transfer basis, these effects do not show up in the pressure drop data.

Hurlburt and Newell [20] have examined the transition between stratified flow and annular flow and have found that a 'Froude rate' parameter indicates a transition between the two flow configurations. For the refrigerant conditions investigated in this study, numerical values for the Froude rate are similar to those for the Froude number. Over an extended range of conditions where circumferential variation of an annular flow's film thickness is of interest, the Froude rate parameter is significantly different and appropriately determines the characteristics of the flow field. The Froude rate parameter is defined as:

$$Ft = [m_v V_v^2/(m_l g D)]^{1/2}. \quad (18)$$

The Froude rate, as seen above, is a ratio related to the vapor's power due to its kinetic energy to the power required to pump liquid from the bottom of the tube to the top of the tube. Alternatively, the Froude rate can be written in terms of refrigerant mass flux and quality.

$$Ft = [x^3G^2/(\rho_v^2 gD(1-x))]^{1/2} \quad (19)$$

The transition between stratified flow and a non-uniform annular film flow is observed when one plots a 'symmetry' parameter; the ratio of average film thickness to the bottom film thickness, versus the Froude rate. Unlike typical flow regime maps, this method for determining the transition between stratified and annular flow regions distinguishes between a 'true' stratified flow and a non-uniform annular film flow. Local film thickness data is required in order to determine the transition point. For air–water systems, the Froude rate shows the transition region in smooth tubes to be near a value of 20. No local film thickness measurement data has been found for refrigerant-type substances. However, assuming similar trends occur, one would expect that a similar level of energy is required from the vapor for distributing liquid around the periphery of the tube.

Figure 11 shows axial tube enhancement factors plotted versus the Froude rate parameter for all experimental data. The plot shows that the region of high enhancement, relative to smooth tubes and the helical tube, occurs between Froude rate values of 1 and 20. The different character of the 75 kg m^{-2} s^{-1} mass flux relative to the higher mass fluxes is clearly seen in Fig. 11. Figure 11 also shows that at Froude rates greater than 20, the relative enhancement is diminished with increasing mass flux. A closer examination of the data indicates that the drop of relative heat transfer in the axial tube on the low quality side occurs at a Froude rate between 1 and 2. Possibly, the axially grooved tube maintains an annular flow configuration that is more efficient than the stratified flow configuration found in smooth tubes. The helical tube appears to maintain a flow configuration similar to that of a smooth tube.

Figure 12 is a parametric plot of Froude rate versus mass flux for R134a at 35°C in an 8 mm inside diameter tube. Lines of constant quality from 0.1 to 0.8 are also marked on Fig. 12. A region between Froude rates of 1 and 20 and mass fluxes from 150 to 450 kg m^{-2} s^{-1} is outlined in order to show the range where an axial tube would have enhancements significantly above those of a helical tube. At the low mass flux range, qualities from 0.2 to 0.8 would be significantly enhanced. Mid-range to higher range mass fluxes of 300 to 450 kg m^{-2} would enhance heat transfer between qualities of 0.1 and 0.6.

It should be noted that an alternative approach to be considered in the data reduction is to not use the equivalent flow diameter when calculating the Froude rate. Instead, if one recognizes that the denominator in the Froude rate is the power required to pump liquid from the bottom to the top of the tube, it might be more accurate when looking at an axial micro-finned tube to consider the power required to pump the liquid from one fin to the next. For example, the tube considered in this study had sixty trapezoidal fins. Therefore, in order to get from the bottom of the tube to the top, the liquid must go over 20 to 30 fins. If one considers only the power required to go from one fin to the next, the total Froude rate would increase by a factor of twenty to thirty.

4. Conclusions

Axial micro-fin grooving shows a region of significant heat transfer enhancement when compared to a similarly

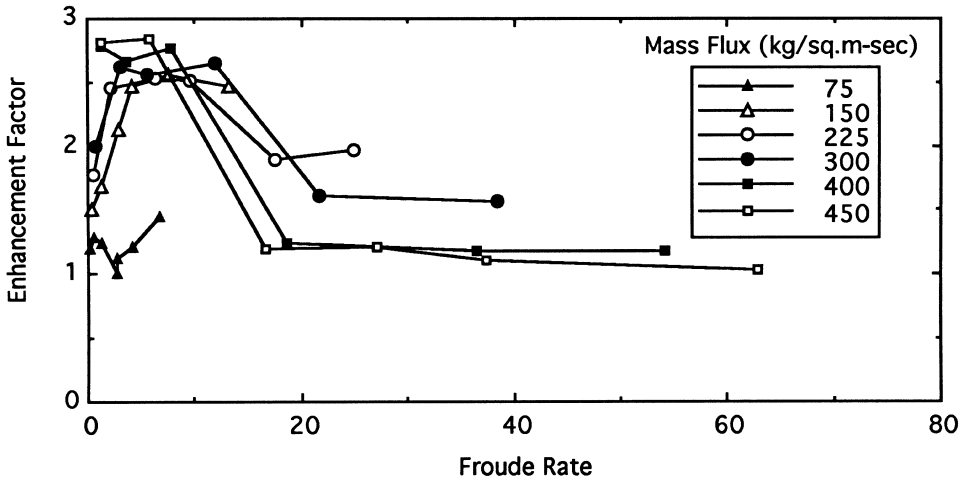

Fig. 11. Plot of axial tube enhancement factors versus the Froude rate parameter for all axial tube data.

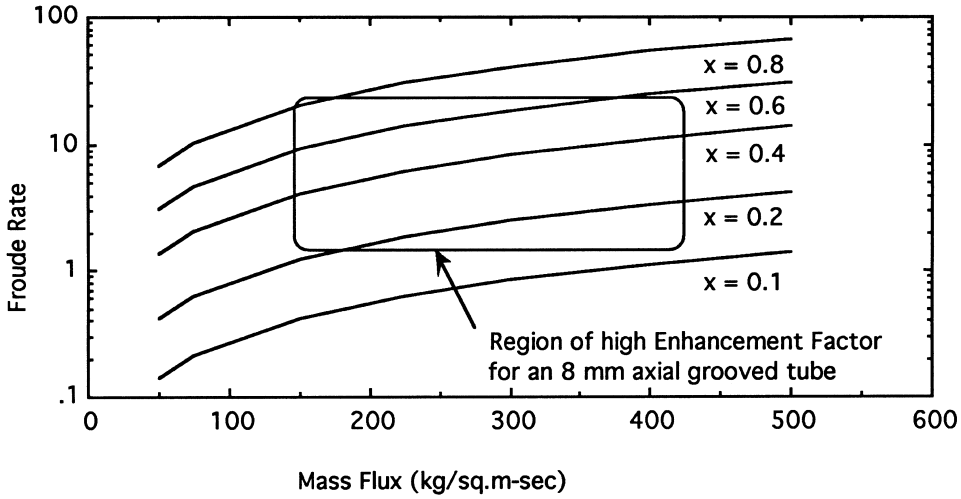

Fig. 12. Plot showing an estimated region for an 8 mm diameter tube in which axial grooves may result in significant increase in performance over helical and smooth tubes.

grooved helical tube. Results show the enhanced heat transfer to be dependent on the mass flux and quality of the refrigerant. A Froude rate parameter provides a basis for correlating the region of enhancement over the mass flux and quality ranges studied. The level of enhancement also appears to be dependent on mass flux. Higher mass fluxes have higher levels of peak enhancement. In terms of pressure drop, the axial tube has a penalty factor that is equivalent to the helical tube.

Future questions to be answered relate to the extension of these results to other conditions. Higher pressure refrigerants (such as R22 with higher vapor densities) and lower pressure refrigerants (such as R123 with lower vapor densities) should be examined. Geometric dependencies should also be examined. The effects of groove geometry and tube diameter variations are unknown. Finally, the effect of oil and its ability to 'clog' grooves should be examined.

Acknowledgements

The authors appreciate the financial support of the UIUC Air Conditioning and Refrigeration Center, an NSF sponsored, Industry supported research center. Modine Manufacturing Company is thanked for special fabrication of axially grooved tubes with dimensions matching their 18° helix tube.

References

[1] R. Chiang, Heat transfer and pressure drop during evaporation and condensation of refrigerant-22 in 7.5 mm and 10 mm diameter axial and helical grooved tubes, AIChE Heat Transfer Symposium, Atlanta, 89 (295) (1993) 205–210.

[2] M.K. Dobson, Heat transfer and flow regimes during condensation in horizontal tubes, Ph.D. thesis, University of Illinois, Urbana, IL, 1994.

[3] M.K. Dobson, J.C. Chato, Condensation in smooth horizontal tubes, Journal of Heat Transfer 120 (1998) 193–213.

[4] S.J. Eckels, M.B. Pate, Evaporation and condensation of HFC-134a and CFC-12 in a smooth and a micro-fin tube, ASHRAE Trans. 97 (2) (1991) 71–81.

[5] M. Luu, A.E. Bergles, Experimental study of the augmentation of in-tube condensation of R-113, ASHRAE Trans. 85 (3) (1979) 132–145.

[6] M. Ponchner, J.C. Chato, Condensation of HFC-134a in an 18° helix angle micro-finned tube, Technical Report, ACRC Report TR-75, University of Illinois, Urbana, 1995.

[7] M. Ponchner, Condensation of HFC-134a in an 18° helix angle micro-finned tube, M.S. thesis, University of Illinois, Urbana, 1995.

[8] J.C. Khanpara, Augmentation of in-tube evaporation and condensation with micro-fin tubes using refrigerants R-113 and R-22, Ph.D. thesis, Iowa State University, Ames, IA, 1986.

[9] L.M. Schlager, M.B. Pate, A.E. Bergles, Evaporation and condensation of refrigerant–oil mixtures in a smooth tube and micro-fin tube, ASHRAE Trans. 94 (1) (1988) 149–166.

[10] L.M. Schlager, M.B. Pate, A.E. Bergles, Evaporation and condensation of refrigerant–oil mixtures in a low-fin tube, ASHRAE Trans. 94 (2) (1988) 1176–1194.

[11] L.M. Schlager, M.B. Pate, A.E. Bergles, A comparison of 150 and 300 SUS oil effects on refrigerant evaporation and condensation in a smooth tube and a micro-fin tube, ASHRAE Trans. 95 (1) (1989) 387–397.

[12] L.M. Schlager, M.B. Pate, A.E. Bergles, Performance predictions of refrigerant–oil mixtures in smooth and internally finned tubes—Part 1: literature review, ASHRAE Trans. 96 (1) (1990) 160–171.

[13] L.M. Schlager, M.B. Pate, A.E. Bergles, Performance predictions of refrigerant–oil mixtures in smooth and internally finned tubes—Part II: design equations, ASHRAE Trans. 96 (1) (1990) 170–182.
[14] B. Sur, N.Z. Azer, Effect of oil on heat transfer and pressure drop during condensation of refrigerant-113 inside smooth and internally finned tubes, ASHRAE Trans. (1991) 365–373.
[15] R.W. Lockhart, R.C. Martinelli, Proposed correlation of data for isothermal two-phase, two-component flow in pipes, Chemical Engineering Progress 45 (1) (1947) 39–48.
[16] H.M. Soliman, On the annular-to-wavy flow pattern transition during condensation inside horizontal tubes, The Canadian Journal of Chemical Engineering 60 (1982) 475–481.
[17] A.M. Souza, J.C. Chato, J.P. Wattelet, B.R. Christoffersen, Pressure drop during two-phase flow of pure refrigerants and refrigerant–oil mixtures in horizontal smooth tubes, ASME HTD 243 (1993) 35–41.
[18] A.M. Souza, J.C. Chato, J.P. Wattelet, Pressure drop during two-phase flow of refrigerants in horizontal smooth tubes, ACRC Report TR-25, University of Illinois, Urbana, 1992.
[19] S.M. Zivi, Estimation of the steady-state void-fraction by means of the principle of minimum entropy production, Journal of Heat Transfer 86 (1964) 247–252.
[20] E.T. Hurlburt, T.A. Newell, Modeling of the evaporation and condensation of zeotropic refrigerant mixtures in horizontal annular flow, ACRC Report TR-129, 1997.